

APPLIED SCIENCES AND ENGINEERING

Magnetic soft micromachines made of linked microactuator networks

Xinghao Hu¹, Immihan C. Yasa¹, Ziyu Ren¹, Sandhya R. Goudu¹, Hakan Ceylan^{1*}, Wenqi Hu^{1*}, Metin Sitti^{1,2,3*}

Soft untethered micromachines with overall sizes less than 100 μm enable diverse programmed shape transformations and functions for future biomedical and organ-on-a-chip applications. However, fabrication of such machines has been hampered by the lack of control of microactuator's programmability. To address such challenge, we use two-photon polymerization to selectively link Janus microparticle-based magnetic microactuators by three-dimensional (3D) printing of soft or rigid polymer microstructures or links. Sequentially, we position each microactuator at a desired location by surface rolling and rotation to a desired position and orientation by applying magnetic field-based torques, and then 3D printing soft or rigid links to connect with other temporarily fixed microactuators. The linked 2D microactuator networks exhibit programmed 2D and 3D shape transformations, and untethered limbless and limbed micromachine prototypes exhibit various robotic gaits for surface locomotion. The fabrication strategy presented here can enable soft micromachine designs and applications at the cellular scales.

INTRODUCTION

Magnetic soft machines that have programmable shape morphing under externally applied magnetic fields would have a transformative impact in developing design strategies for soft robots (1–3), mechanical metamaterials (4, 5), lab/organ-on-a-chip devices (6, 7), and minimally invasive medical devices (8–10), due to their safe/gentle interaction with the environment, wireless and robust controllability, large design space for magnetic programming, and fast response time to external magnetic fields (11–19). Such design strategy entails preprogramming of local magnetic domains inside a soft polymer body, such that the magnetic field-based torques applied on the magnetic domains can deform the body in prescribed directions (16–19). In these designs, pre-alignment of a network of micromagnets within the polymer body can form a sufficiently high net local magnetic torque vectors in desired orientations. Nevertheless, as the body size goes down to cellular length scales ($<100\ \mu\text{m}$), the size of magnetic domains becomes comparable to the size of individual micromagnets, e.g., magnetic microparticles. The lack of robust methods to control two-dimensional (2D) or 3D position and magnetic orientation of the individual micromagnets precisely has limited the development of magnetic soft machines down to the micrometer scale. Previously, magnetic microparticles have been demonstrated to spontaneously form superstructures under applied light, magnetic or electric fields (20–24), and the assembled structures, such as chains (25), wheels (26), gears (27), and asters (28), enabling locomotion under dynamic magnetic fields. However, linking the micromagnets has only been demonstrated so far as very basic soft micromachines, including 1D DNA-linked isotropic microparticles (29), 1D nanowires with flexible joints (30–32), and 2D thin-film micromagnets with hinge springs (33), with no magnetic programmability or fabrication of 3D structures.

¹Physical Intelligence Department, Max Planck Institute for Intelligent Systems, 70569 Stuttgart, Germany. ²Institute for Biomedical Engineering, ETH Zürich, 8092 Zürich, Switzerland. ³School of Medicine and College of Engineering, Koç University, 34450 Istanbul, Turkey.

*Corresponding author. Email: sitti@is.mpg.de (M.S.); ceylan@is.mpg.de (H.C.); wenqi@is.mpg.de (W.H.)

To address these challenges, we propose an assembly-based fabrication strategy, where we bring together electromagnetic steering control to position and orient individual microactuators and two-photon polymerization to form soft or rigid links or structures between microactuators. We use Janus microparticles as model magnetic microactuators, because they could be soft magnetic and monodisperse in a wide range of sizes and materials (34–36), and their inherent magnetic shape anisotropy allows magnetic programmability. Specifically, we program the orientation of the easy axis of magnetization of each microactuator at a desired position by magnetic field-based control and link the microactuators with soft hydrogel links or structures. We present the robustness and precision of such soft micromachine fabrication strategy by demonstrating various 1D, 2D, and 3D deformable magnetic soft structures. We first demonstrate single-microactuator cantilevers with mechanical anisotropy for selective actuation and 1D deformation and then demonstrate microactuator networks to build soft micromachines with 2D and 3D programmable shape deformations. Next, we show untethered limbless and limbed micromachines that exhibit a variety of robotic gaits for soft-bodied surface locomotion under controlled magnetic fields. The fabrication strategy presented herein can greatly extend possibilities toward soft micromachine designs with sub-micrometer features and diverse functions as well as the ability to integrate multimaterial components/structures and distributed magnetic actuators at the micrometer scale.

RESULTS

Fabrication methodology

We integrate an electromagnetic coil setup in a commercial two-photon polymerization system (Nanoscribe GmbH) to apply 3D magnetic fields to control locations of microactuators as well as encode the easy axis, i.e., orientation, of microactuator magnetization (fig. S1). Before the sequential assembly of soft micromachines, the microactuators in the form of spherical Janus microparticles are prepared by the directional magnetron sputtering deposition of permalloy (Py) (60 nm thick) and then gold (Au, 15 nm thick) thin films on silica microspheres. The Janus particles are finally coated with

Copyright © 2021
The Authors, some
rights reserved;
exclusive licensee
American Association
for the Advancement
of Science. No claim to
original U.S. Government
Works. Distributed
under a Creative
Commons Attribution
License 4.0 (CC BY).

polyethylene glycol (PEG) on the Au layer to reduce nonspecific adhesion as well as to ensure biocompatibility. Thus, the half-site of the Janus particles is metallic (PEG-coated Au) and the other half-site is silica.

Figure 1A presents the fabrication schematics and capability of the proposed strategy, which enables soft micromachines with assembled soft and rigid materials by two-photon polymerization (i.e., 3D microprinting) and embedded microactuators at specific 2D positions and orientations. General fabrication steps are shown in Fig. 1B (for the detailed assembly procedure, see Materials and Methods). First, the microactuator is rolled on the glass substrate to reach a target position precisely under a rotating magnetic field (fig. S2). Second, because the easy axis of the microactuator is aligned with the applied magnetic field (H) direction due to the exerted magnetic torque τ_m (fig. S3), the microactuator orientation is controlled by rotating it in roll and pitch directions to reach the target easy axis at that position by applying H . Third, the microactuator is temporarily anchored on the substrate by two-photon polymerization. The anchoring sacrificial material is PEG diacrylate (PEGDA) hydrogel. Fourth, a ring-shaped holding polymeric structure (IP-L, Nanoscribe GmbH) is 3D-microprinted on the anchored microactuator to be able to connect it to 3D-printed microstructures or links. The above four steps are sequentially repeated for each microactuator until all microactuators are fixed on the substrate temporarily in the desired positions and orientations. Next, 3D structures

or links between all fixed microactuators are 3D-microprinted using a soft (e.g., gelatin hydrogel) or hard polymer. Last, the fabricated soft micromachine is released from the glass substrate by soaking it in deionized (DI) water. The anchors of PEGDA swell in water so that the samples can be detached from the substrate. Here, a laser assistance is helpful to release the samples because the laser heating at the metallic site can produce microbubbles that can push the samples away from the substrate. Then, the released device can be actuated by external magnetic fields in the given operation space.

A bending hydrogel cantilever beam device

As the very basic 1D-deforming soft microdevice, we first assembled 3D-microprinted hydrogel cantilever beams with a Janus microparticle at its tip (Fig. 2A) in two different particle and beam orientations to induce both in-plane and out-of-plane bending (Fig. 2A, i). For enabling in-plane bending, the left particle has the easy axis approximately at 45° away from the x axis in the anticlockwise direction. The cross section of the beam connecting the microparticle and the anchoring post is $2 \times 4 \mu\text{m}^2$ (width \times height) to the nominal geometry of 3D microprinting. For the out-of-plane bending, the easy axis of the right particle is approximately perpendicular to the ladder-shaped hydrogel beam. The cross section of the ladder-shaped beam is $4 \times 0.5 \mu\text{m}^2$ (width \times height), and the width of the rungs of the ladder is $1 \mu\text{m}$. Note that, to print soft beams on a single particle, the ring structure and the releasing steps shown in Fig. 1B are not necessary.

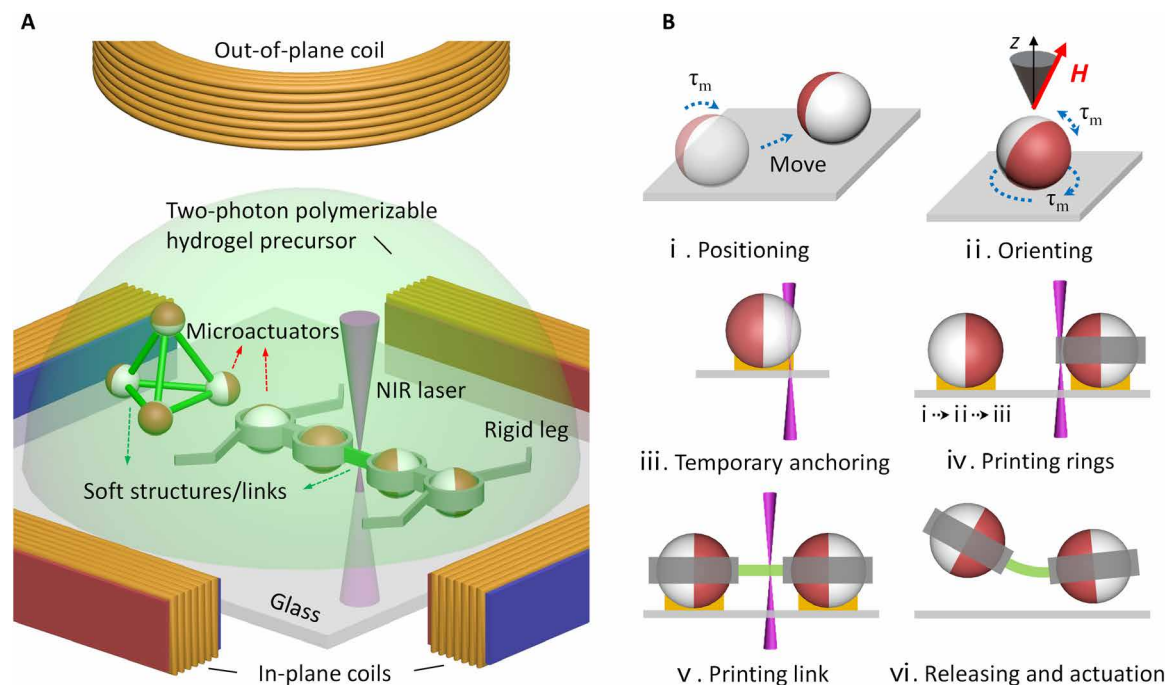


Fig. 1. Soft micromachine fabrication strategy. (A) Fabrication process schematics of soft micromachines using a two-photon polymerization (3D microprinting) system with an integrated electromagnetic coil setup. Microactuators (soft magnetic, monodisperse, and spherical Janus microparticles) are manipulated magnetically to reach a desired position and orientation and fixed there temporarily using 3D microprinting. Soft and rigid materials can be 3D-printed on a fixed microactuator to link it with other fixed microactuators. (B) Schematic details of the fabrication process for an example two-particle chain: (i) The first microactuator is positioned to a specific location by surface rolling. (ii) The microactuator's orientation is controlled by a rotating magnetic field H . (iii) The oriented microactuator is anchored temporarily on the glass substrate. (iv) A ring-shaped holding structure is 3D-printed to be able to bond other 3D-printed microstructures at the microactuator's metallic site. The above four steps are repeated for the second microactuator. (v) A soft (i.e., gelatin hydrogel) or rigid link between the microactuators is 3D-printed. (vi) The final soft micromachine is released (with laser assistance) from the glass substrate by soaking it in deionized (DI) water. Then, the released device is actuated by external magnetic fields generated by the electromagnetic coils in the given operation space.

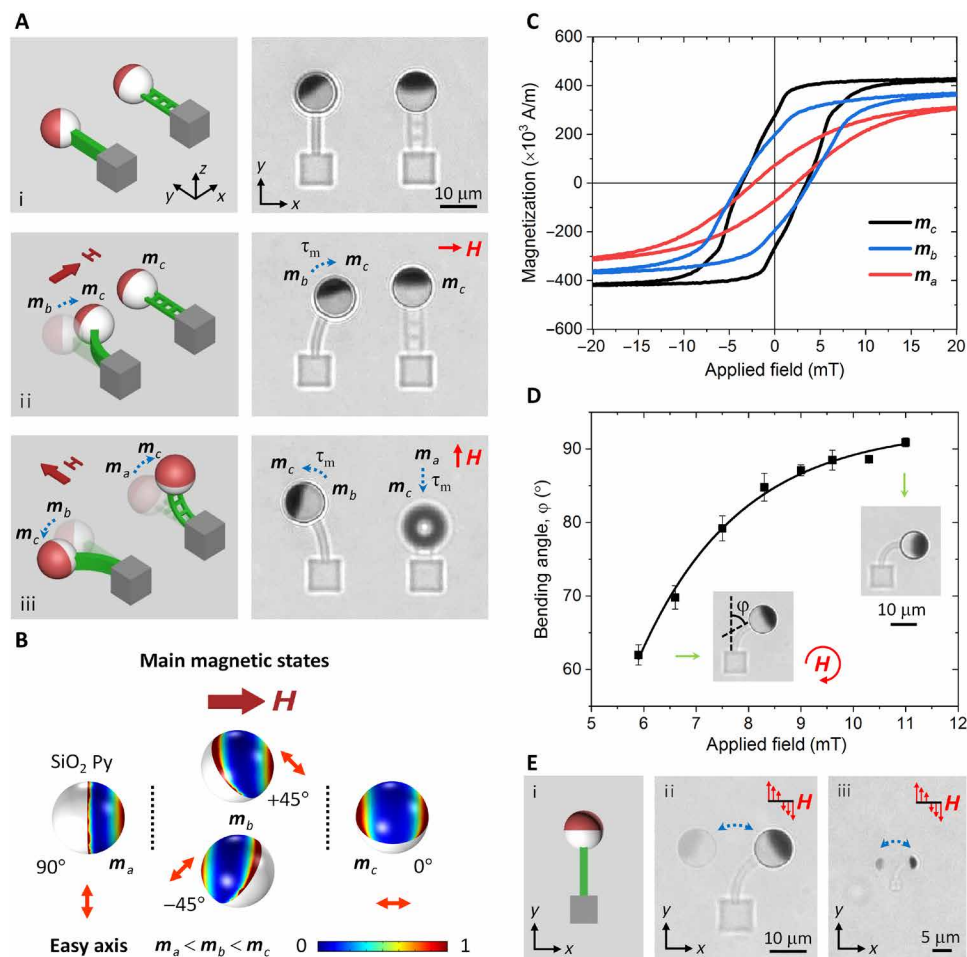


Fig. 2. Characterization of the fabricated hydrogel cantilever beams. (A) The particle orientation and cantilever geometry determine bending directions under an applied field. (i) Rectangular and ladder hydrogel beams are printed on microactuators with approximate 45° and 90° angles to the easy axis, respectively. (ii) Under the applied field in the x axis (9 mT), the rectangular beam presents an in-plane bending to the right, but the ladder beam does not have bending owing to the particle already in the m_c state. (iii) Under the applied field in the y axis, the rectangular beam presents an in-plane bending to the left, and the ladder beam presents an out-of-plane bending to lift the particle. (B) Main magnetic states of microactuators, m_a (90°), m_b ($+45^\circ$ or -45°), and m_c (0°). Magnetic energy density on microactuators (10- μm diameter) are performed under an applied field (10 mT). The multiplication factor for the color bar is 110 J/m^3 . (C) Magnetic hysteresis loops of microactuators (10- μm diameter) with different easy-axis orientations, 90° , 45° , and 0° , respectively, to the applied field. (D) Maximum bending angles of the particle cantilever under in-plane rotating fields in clockwise direction at 0.5-Hz frequency. (E) Oscillation of different-sized particle cantilevers [schematic (i)] under an oscillating field (from $+9$ to -9 mT at 1.2-Hz frequency). The particle diameters are 10 μm (ii) and 3 μm (iii).

This is because we just need to link hydrogel at the silica site of the Janus particle rather than the metallic site, where a laser-induced heat would be generated that can affect the hydrogel polymerization during printing.

Although the particle orientations can be aligned in any angle, we only use main magnetic states (m_a , m_b , and m_c) for demonstrations of the device shape transformation in this work (Fig. 2B). m_a , m_b , and m_c states represent three typical magnetizations of the individual microactuators when their easy axis (the direction of double-sided arrows) is subject to the H direction 90° , 45° , and 0° , respectively. The symmetric magnetic energy density at two poles on the magnetic cap indicates that the m_c state is in stable equilibrium under the applied field. Furthermore, the magnetization increases when the magnetic caps are oriented from perpendicular (m_a) to parallel (m_c) to the H direction (Fig. 2C). It demonstrates that the easy axis of the particle is parallel to the magnetic cap. Therefore, when H is not

parallel to the magnetic cap, the microactuators would induce a torque and rotate toward the m_c state.

As shown in Fig. 2A (ii), when H (9 mT) along the x axis is turned on, the left particle beam bends to the right (from m_b toward the m_c state) while the right particle beam remains still as the particle can retain the m_c state. When H (9 mT) along the y axis is turned on, the left particle beam bends to the left (from m_b toward the m_c state) and the right particle beam bends up (Fig. 2A, iii, and see movie S1). The large deformation of a cantilever beam can be observed under an applied rotating field, because the magnetic torque is increasing until the phase lag between the particle easy axis and the applied field direction reaches the maximum. The maximum bending angles of the rectangular hydrogel cantilever (a 10- μm particle at the tip for the in-plane bending case) are characterized experimentally under applied in-plane rotating fields at 0.5-Hz frequency in the clockwise direction, as shown in Fig. 2D. Furthermore, we develop

a model-based simulation to predict the bending angle of the hydrogel beam, which is derived from the evaluation of the magnetic torque on a Janus microparticle (fig. S4 and see Materials and Methods) and the mechanical property of the 3D-microprinted hydrogel structures (figs. S5, A to C, and S6). The simulation results agree well with the experimentally characterized bending angles under the varied static magnetic fields (fig. S5D).

In addition, different-sized microparticles with diameter down to 1 μm have been tested for printing hydrogel cantilevers to the in-plane 1D bending case. The decrease of the beam cross section is proportional to the diameter of the microparticles. Figure 2E shows that the microparticles are printed with cantilevers perpendicular to the easy axis (Fig. 2E, i) and can oscillate from the left to the right side under an oscillating field H_y from +9 to -9 mT at 1.2-Hz frequency (movie S2). The particle diameters are 10 μm (Fig. 2E, ii), 5 μm (fig. S7A), 3 μm (Fig. 2E, iii), and 1 μm (fig. S7B). It indicates that the microparticles have preferred magnetization direction in the easy-axis plane, which is caused by the initial magnetization procedure in the atomic crystal alignment of the ferromagnetic thin film. The Py magnetic layer on the Janus particles is a ferromagnetic material (fig. S8A), and fig. S8B shows the ferromagnetic hysteresis loops of the Janus particles with different sizes along the easy-axis plane. The magnetic spins in the Janus cap gradually vary with different applied fields (fig. S9). However, the magnetic shape anisotropy of the microparticle dominates the bending direction of the linked hydrogel beam, which is designed with a mechanical anisotropy rather than the preferred magnetization to induce the torque. The rheological investigation of the hydrogel shows low values of $\tan\delta = G''/G'$ (G'' and G' are storage and loss modulus, respectively) at varied angular frequencies (fig. S10), which demonstrates that the elastic property of the hydrogel dominates during the dynamic actuation.

1D and 2D soft robotic chains

Untethered 1D and 2D robotic chains with multiple encoded Janus particles can have dynamic shape deformation and locomotion under varying magnetic fields as well as the functional ability of manipulating objects. Figure 3A shows that the easy axis of two microactuators is along the x and y axis, respectively. When turning on H in the y direction, the two microactuators are not in stable equilibrium, because they are in m_c and m_a magnetization states, respectively. As shown in the landscape of magnetic energy density over the oriented particles (Fig. 3A, i), the left particle (m_c) induces a symmetric energy along the applied field direction, but the right particle (m_a) induces an asymmetric energy. Therefore, it would be turned 90° in the out-of-plane direction under the applied field, resulting in the two particles both in m_c states as shown in Fig. 3B. As an example, the fabrication processes of the two-microactuator chain are shown in movie S3, and fig. S11 shows the design details of the anchoring pillars and the ring-shaped holding structures.

Furthermore, this kind of encoded chain can be actuated for dynamic locomotion under varying magnetic fields (fig. S12), but it does not exhibit a stable locomotion in the open space, because the structural element built with only one microparticle is not sufficient to hold the orientation of the structure when another concatenating microparticle functions as an actuator. Therefore, we assemble two particles, which are always in the same orientation (m_c state) under the varying magnetic fields as the structural element, to increase the viscous drag induced by the surrounding fluid and the friction force

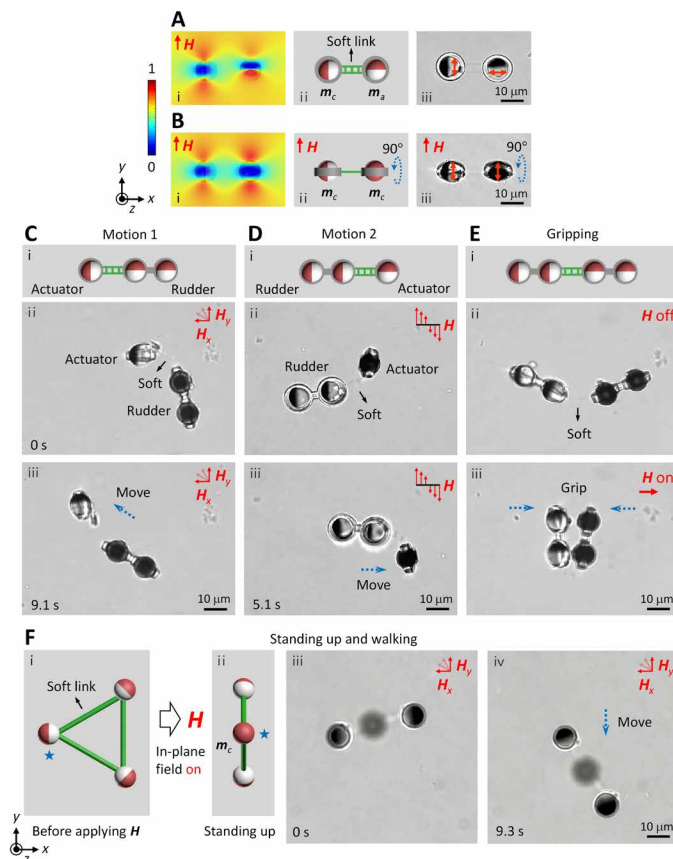


Fig. 3. Soft robotic particle chains. (A and B) Magnetic energy density over the oriented particles (i), schematic of the oriented particles (ii), and the optical microscopy image of hydrogel-linked particles (iii) from the left to the right side, respectively. The red arrow represents the magnetic field direction. The multiplication factor for the color bar is 41 J/m^3 . After applying an in-plane magnetic field in the y axis, the chain with two microactuators at the m_c and m_a states (A) rotates 90° in the yz plane to the state of both at the m_c state (B). (C) Hydrogel-linked particles with the specific orientations (i) show a surface locomotion (ii and iii) under an oscillating field between H_x and H_y (9 mT at 3-Hz frequency). (D) Hydrogel-linked particles with the specific orientations (i) show locomotion (ii and iii) under an oscillating field along one direction (amplitude 9 mT at 2-Hz frequency). (E) Gripping performance of the hydrogel-linked particles under an applied static field (9 mT). (F) A triangle structure with three encoded particles at the apexes can stand up (i and ii) under an applied in-plane field. The standing structure exhibits walking locomotion (iii and iv) with two particles as one pair of legs and the third particle (at the m_c state) controlling the balance, under an oscillating field between H_x and H_y (9 mT at 0.5-Hz frequency).

from the contacted substrate (37). As shown in Fig. 3C, the microparticle (m_c state initially) can be an actuator for propulsion toward the upper left side under an oscillating field between H_x and H_y , when the easy axis of other two microparticles (m_a state initially) aligns with the xy plane as a rudder to hold the structure. On the other hand, the microparticle (m_a state initially) can also function as an oar for propulsion (m_c state initially). With an oscillating field along the y axis, it moves to the right side (Fig. 3D and movie S4). Here, the propulsion mechanism is similar to the undulation motion of nanowires with soft links (32).

Figure 3E shows that the encoded chain also has a gripping capability. The gripper is designed to have two encoded arms in m_a and m_c initial states, respectively, and each arm has two microparticles

with the same orientation, which could enhance the gripping torque. When the field H_x is on, the two arms grip and release when the field is off (movie S5). Here, the gripper-cargo complex could be pulled by a magnetic spatial gradient for controlled locomotion and position control, which is possible by using a proper magnetic actuation coil setup, as a future work. If the two microparticles (m_c state initially) are assembled together, the rigid link can assist to manipulate a single cell (fig. S13 and movie S6). Furthermore, a triangle structure with three encoded microparticles at the apexes can stand up and exhibit a walking locomotion with two microparticles as one pair of legs and the third microparticle controlling the balance (Fig. 3F and movie S7).

2D microactuator networks

We also show the capability to make soft micromachines with 2D network configurations toward advanced 2D or 3D shape morphing behavior and soft robotic locomotion capability. Specifically, we design a 3 by 3 array of microactuator network, as shown in Fig. 4A. As the notable feature of this design, the array with rectangular hydrogel beams encodes the easy axis of each microactuator with alternating 45° along the beams. When H is turned on, this design could present an active behavior to shrink in both x and y directions. This mimics the typical feature of auxetic microstructures with negative Poisson's ratio (movie S8). Figure 4A (ii to iv) shows the experimental results under the applied fields H with 10 mT (simulation see in fig. S14). This structure shrinks 9.1% in the x axis and 9.2% in the y axis. In Fig. 4B, another design is demonstrated. The design shown in

Fig. 4B (i) contrasts Fig. 4A (i) by its soft link design. With the design in Fig. 4B (i), the microactuators are allowed to bend into the $+z$ direction. When a rotating 3D field H (8.1 mT) is applied, where the field direction is tilted a little bit to the $+z$ direction (8.5°) from the xy plane, the network will twist and wobble along with H (movie S9). To understand this dynamic shape deformation, figure S15A shows that if the applied field H is in the xy plane only, the opposite cantilevers can both bend to the $+z$ direction. However, if H is tilted to the z axis, one of the opposite cantilevers would still bend to the $+z$ direction, but another one would twist (fig. S15, B and C).

2D-legged mobile microrobots

To demonstrate the fabrication versatility and untethered soft microrobotic design possibilities, soft micromachines with rigid or soft legs for different walking gaits have been developed. Figure 5A shows the assembled lizard-like walking robot with four encoded microactuators (the easy axis has 45° along the robot body), two pairs of rigid legs, and a hydrogel body with a rectangular cross section (1- μm width and 4- μm height) to provide flexibility in the body. Under an oscillating field along the y axis (from 9 to -9 mT at 1-Hz frequency), the two pairs of legs alternately strike the ground, resulting in locomotion of lizard-like walking, as shown in Fig. 5(B to D) (movie S10). Figure 5E shows the assembled robot with three pairs of soft legs (rectangular cross section with 1- μm width and 4- μm height) and a rigid body. It also presents programmable robotic gaits under an oscillating field (Fig. 5, F to H, and movie S11).

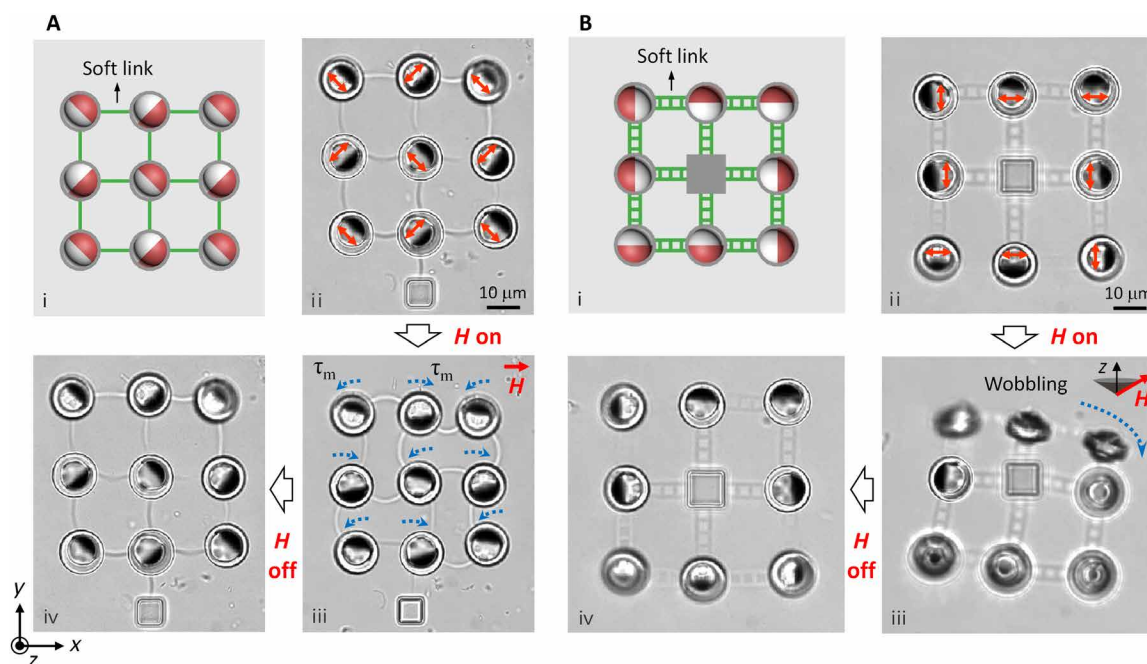


Fig. 4. Soft robotic 2D particle networks having 2D and 3D shape deformations. (A) An auxetic microstructure with negative Poisson's ratio can be observed in a 3 by 3 array microactuator network. The easy axis of each microactuator is encoded with alternating 45° along the beams indicated by the double-sided arrows (i and ii). The cross-sectional dimensions of the rectangular hydrogel beam are 1- μm width and 4- μm height. By applying a magnetic field (10 mT) on and off, the network presents programmable shape transformations (iii and iv). (B) A microstructure of a 3 by 3 array network with ladder-like hydrogel beams presents a wobbling motion under a rotating field. The easy axis of each microactuator is encoded orderly perpendicular and parallel to the beams indicated by the double-sided arrows (i and ii). The cross-sectional dimensions of the ladder-like hydrogel beam are 1- μm ladder beam width, 4- μm overall width, and 0.5- μm height. By applying a rotating 3D field H in clockwise direction (8.1-mT field strength, tilting angle in the $+z$ axis from the xy plane is 8.5°, and 0.6-Hz frequency), the encoded network presents periodic 3D shape deformations (iii and iv).

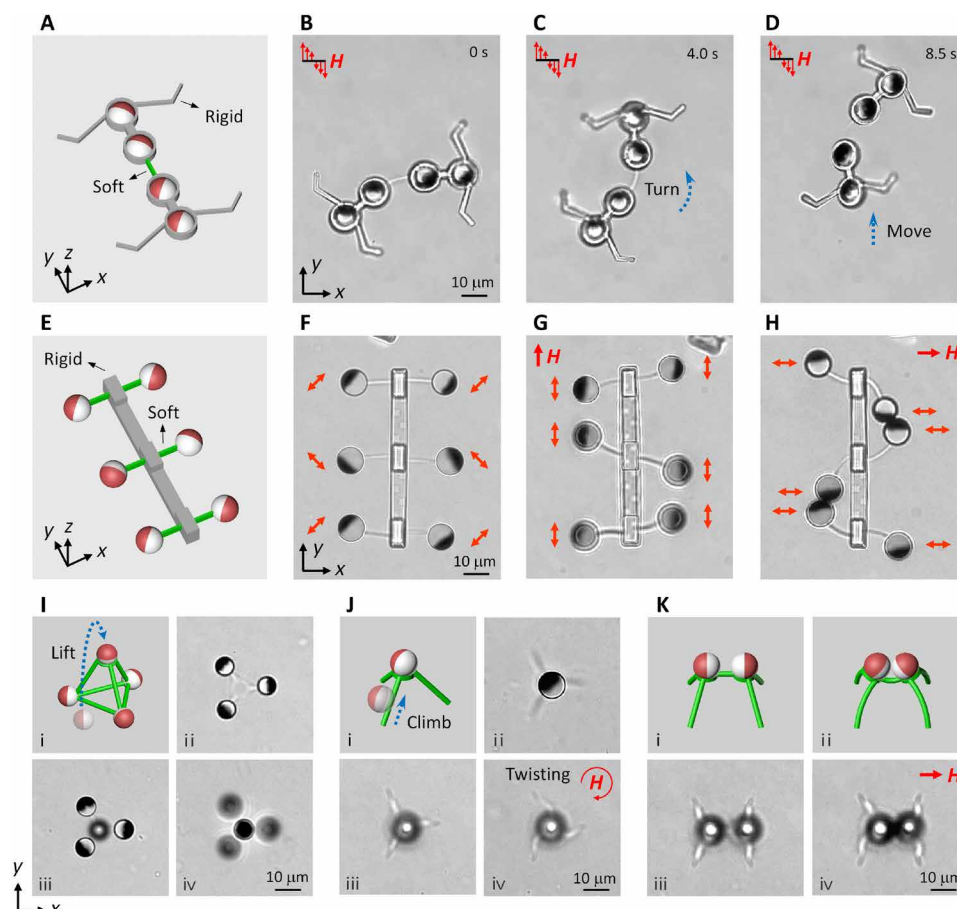


Fig. 5. Two-legged soft microbot demonstrations and fabrication of a tetrahedron array toward future 3D soft micromachine configurations. (A to D) A lizard-like walking robot with four rigid legs presents a surface locomotion under an oscillating field (from +9 to −9 mT at 1-Hz frequency). (E to H) Soft-legged robot presents programmable robotic gaits under an alternating field (9 mT). (I) Tetrahedron array of four oriented particles with 7- μm diameter. Particle levitation is controlled by the applied magnetic gradient fields in the vertical (z) direction. Schematic (i), printed 3D hydrogel structures on three encoded particles (ii), the optical microscopy image of focusing on the three particles (iii), and the optical microscopy image of focusing on the lifted/levitated particle (iv). (J) 3D configuration of a particle with 10- μm diameter by rolling motion along the hydrogel beam. Schematic (i), the optical microscopy image of focusing on the particle (ii), the optical microscopy image of focusing on the hydrogel beams (iii), and actuation (iv) under a rotating in-plane field (12.5 mT). (K) Two oriented particles show 3D shape changes of hydrogel beams under an applied field. Schematics (i and ii), the optical microscopy image of focusing on the hydrogel beams without applied fields (iii), and with actuation (iv) under an applied field (12.5 mT).

Tetrahedral pyramid soft micromachine toward 3D configurations

While the above demonstrations show 2D microactuator network configurations, the microactuators can also be positioned in 3D space as a preliminary step toward 3D future configurations, either by levitating the microactuators in the vertical axis using 3D gradient fields or by a rolling motion along the 3D-microprinted hydrogel beam. For example, Fig. 5I shows a tetrahedral pyramid with encoded four particles at the apexes. To assemble the fourth particle on the top apex of the 2D network, a gradient force in the +z direction was used to lift the microactuators to the top of the 3D-microprinted hydrogel structure (movie S12). In this demonstration, each particle has a nominal 7- μm diameter, $m = 0.92 \times 10^{-12} \text{ A}\cdot\text{m}^2$ (in saturation along the easy axis), and the net gravitational force is 1.49 pN (subtracting buoyancy force from gravity force in water). For a particle with a nominal 10- μm diameter, m is $1.88 \times 10^{-12} \text{ A}\cdot\text{m}^2$ and the net gravitational force is 4.36 pN. It requires around 2.9 times higher field gradients in the +z direction to lift up in comparison with the 7- μm particle. Such high magnetic gradient is a burden to our

current coil setup. As an alternative method, larger particles can be rolled along the printed hydrogel beam to reach the top apex, as shown in Fig. 5J (movie S13). When a rotating in-plane field of 12.5 mT in clockwise direction is applied, the 3D-microprinted hydrogel beams show obvious 3D deformations (Fig. 5J, iv). Last, two encoded microactuators in 3D space can induce more complex shape transformations on multiple hydrogel beams (Fig. 5K). Note that the experiments are performed inside the gelatin precursor here because the water development process may deform the 3D-microprinted hydrogel structures.

DISCUSSION

Magnetic spherical Janus particles are used to program the magnetization profile of each microactuator based on their magnetic shape anisotropy, and they serve as the building blocks to form soft hydrogel micromachines to achieve programmable shape transformations. The fabrication speed is limited by the one-by-one serial assembly procedure of each microactuator and multistep procedures for

linking the microactuators. However, such limitation can be mitigated by using other assembly methods, such as electric fields (24), or using variable building blocks, which can be synthesized to diverse shapes, such as cubes, rods, ellipsoids, faceted polyhedrals, and different patterned particles (38, 39). To add more functions to the fabricated soft micromachines, multiple stimuli-responsive materials or methods could be integrated together for actuation, sensing, and cargo delivery simultaneously (8–10, 40–45). The proposed hierarchical assembly strategy using two-photon polymerization enables 3D configurations of building blocks, which could generate more versatile shape deformations and functions. As potential future applications, the fabricated microactuator networks with 2D/3D shape transformations could be used in active shape morphing and reconfigurable extracellular matrices for tissue engineering and wound healing and wireless soft microgrippers for manipulating fragile microobjects, such as cells. In addition, such soft micromachine designs and fabrication process can be extended to biocompatible magnetic materials, such as ferromagnetic iron platinum (FePt) nanoparticles (46–48) and Janus microparticles, for future biomedical applications.

MATERIALS AND METHODS

Experimental setup

To steer the Janus particles, we integrated an electromagnetic coil setup in a commercially available direct laser writing system (Photonic Professional, Nanoscribe GmbH, Germany), as shown in fig. S1. The electromagnetic coil setup is composed of five independent electromagnets controlled by custom electronics. The coils are able to apply the magnetic field up to 18 mT at the center (the origin of the global coordinate system). The coil setup can be fixed onto a sample holder for the Nanoscribe system. The out-of-plane field electromagnet can be loaded from the top in the Nanoscribe system. Furthermore, the coil setup allows using 12 mm by 12 mm glass substrates for fabrication, but the printing space is limited by a polydimethylsiloxane (PDMS) (with 15:1 w/w ratio of the monomer and the cross-linking agent) well on the substrate that produces a closed environment with another disk glass on the top (8-mm diameter) to prevent evaporation of the printing material precursor.

Fabrication and characterization of Janus particles

Silica (SiO₂) particles were purchased from microParticles GmbH. They are nonporous and have a density of 1.85 g/cm³. To fabricate Janus particles, first, self-assembled monolayers of SiO₂ particles were prepared by the following procedures: (i) The cleaning of glass substrates includes ultrasonication in acetone, drying by nitrogen gas flow, and treatment in oxygen plasma for 5 min. (ii) A particle/water solution was dropped on the cleaned glass substrate. (iii) The droplet evaporates in a titled box. Sufficient coverage of particle monolayers on the substrate can be obtained by varying the particle concentration in the solution, the titled angle, and the droplet size. (iv) Magnetron sputtering was carried out at room temperature for the deposition of Py (Ni₈₁Fe₁₉, 60 nm) and gold (15 nm) thin films on the particle monolayers. Deposition conditions were as follows: base pressure 3.6 × 10⁻⁶ mbar, Ar sputtering pressure 5.7 × 10⁻² mbar for the Py film, and 3.7 × 10⁻² mbar for the gold film. (v) The substrate with particles was immersed in DI water mixed with PEG thiol (100 mg/ml) for 12 hours on a vibrating platform before releasing particles from the substrate by ultrasonication. This PEG layer coated on the gold film could reduce nonspecific adhesions and ensures

biocompatibility. Furthermore, the magnetization property of the particles was characterized on the substrate with the particle monolayer by a vibrating sample magnetometer (VSM; MicroSense, EZ7).

Preparation of hydrogel precursors

Soft polymer gelatin precursor was prepared and used fresh right before printing. Gelatin methacryloyl (100 mg/ml), lithium phenyl (2,4,6-trimethylbenzoyl) phosphinate (30 mg/ml), and iron oxide nanoparticles (concentration 0.5 mg/ml) coated with PEG amine of 50-nm hydrodynamic size (Chemicell GmbH, Germany) were mixed in ultrapure water with vortex mixing and ultrasound sonication. PEGDA precursor was prepared using PEGDA (molecular weight 575, Sigma-Aldrich) and a photoinitiator [(3 weight % (wt %)), 2-hydroxy-4'-(2-hydroxyethoxy)-2-methylpropiophenone (Irgacure 2959, Sigma-Aldrich), with vortex mixing and ultrasound sonication.

Detailed assembly procedures

First, PEGDA precursor mixed with Janus particles was dropped into the PDMS chamber attached to a cleaned glass slide, which was mounted by Fixogum at the center of the coil setup (fig. S1D). Then, the fabrication was carried out. Nanoscribe system with a ×63 oil-immersion objective (NA 1.4) was used for 3D microprinting via two-photon polymerization. As illustrated in Fig. 1B, the procedures of positioning, orienting, and temporary anchoring of Janus particles were executed in PEGDA precursor. Laser power and galvanometric mirror *x*- and *y*-scanning speeds were optimized for printing at 11 mW and 3000 μm/s, respectively. The development of PEGDA was performed in the PDMS chamber using isopropanol (change isopropanol solution in the chamber five times for 5 min for a good development). Second, a resin droplet (IP-L, Nanoscribe GmbH) was dropped into the PDMS chamber for printing ring-shape holding structures as well as rigid links and legs. Laser power and galvanometric mirror *x*- and *y*-scanning speeds were optimized for printing at 22.5 mW and 40,000 μm/s, respectively. The development of IP-L was performed in the PDMS chamber using isopropanol (change isopropanol solution in the chamber five times for 10 min for a good development). Last, we dropped the gelatin precursor in the PDMS chamber for printing soft structures/links. Laser power and galvanometric mirror *x*- and *y*-scanning speeds were optimized for printing at 16 mW and 3000 μm/s, respectively. The development of gelatin was performed in the PDMS chamber using DI water. Thus, the anchors of PEGDA got swelling in DI water, and the samples can be detached from the substrate. Here, laser assistance is helpful to release the samples because the laser heating at the metal layer site can produce bubbles to push the samples away from the substrate (see movie S3, fabrication procedures). Laser power and galvanometric mirror *x*- and *y*-scanning speeds were optimized for assistance to release samples at 30 mW and 5000 μm/s, respectively.

However, ring-shaped holding structures and releasing steps shown in Fig. 1B are not necessary in fabrication of the single-particle cantilevers. This is because we just need to print hydrogel at the silica site of the Janus particles, not at the metal layer site, which generates a laser-induced heat to affect the hydrogel polymerization. Thus, it is possible to directly print the soft beams on an oriented particle, which is controlled by the processing field. In addition, all actuation experiments were carried out in the electromagnetic coil setup integrated with the Nanoscribe two-photon polymerization system.

Numerical evaluation of the magnetic torque on a Janus microparticle

As shown in fig. S4A, when the easy axis (y axis) of Janus particle magnetization is not aligned with the direction of the applied magnetic field (\mathbf{H}) having an angle θ ($0^\circ < \theta < 90^\circ$), the particle would generate a clockwise self-rotation toward its easy axis to align with the field direction. The induced magnetic dipole moment (\mathbf{m}) forms an angle β from the field direction, and the angle β can be experimentally measured from the angle-dependent magnetic moment (fig. S4B) similar to the magnetic measurements of the ferromagnetic nanorods in (49), where

$$\beta = \arccos(m_h/m_s) \quad (1)$$

where m_h is the magnetic moment along the field direction and m_s is the saturated magnetic moment when the field direction is along the Janus particle easy axis. The ferromagnetic thin film (60-nm thickness) on the particle forms a large magnetic shape anisotropy, which causes the magnetic moment to be effectively pinned in the thin-film plane. Therefore, the magnetic torque on a particle ($\vec{\tau}_m$) can be represented as the torque on the ferromagnetic nanorods (49)

$$|\vec{\tau}_m| = |\mu_0 \vec{m} \times \vec{H}| = \mu_0 m_s H \sin\beta \quad (2)$$

where μ_0 is the permeability of vacuum, \vec{m} is the particle magnetic moment, and \vec{H} is the applied magnetic field.

Characterization of the gelatin hydrogel

Rheological analysis of bulk gelatin methacryloyl gel (10 wt %) was performed using a TA Discovery Hybrid HR-3 rheometer with a 25-mm parallel-plate configuration in the oscillatory mode. The gel was prepared in the same way as that for the two-photon polymerization precursor. The precursor was exposed under 365-nm UV light for 30 min. The cylindrical gel with a 25-mm diameter and 1-mm thickness (gap distance) was placed on the lower plate of the rheometer. Frequency sweep test was performed under constant strain, 0.01%, with ramping from 0.1 to 100 rad/s. Next, nanoindentation analysis was performed by an atomic force microscope (AFM) (NanoWizard 4, JPK Instruments). We used the AFM cantilever with a spherical silica particle tip with 5 μm diameter (NanoAndMore, GmbH), which had a spring constant of 0.212 N/m. The gelatin block was prepared using the same cross-linking parameters with the 3D-printed hydrogel micromachines. Laser power and galvanometric mirror x - and y -scanning speeds were 16 mW and 3000 $\mu\text{m/s}$ for 3D printing, respectively.

Finite element method simulations

Finite element simulations were performed in COMSOL Multiphysics software. It used experimentally measured material properties to model magnetic shape anisotropy induced by oriented Janus particles. Specifically, we used the magnetization curve of Py thin film with 60-nm thickness (fig. S8A), from which we obtained the saturation magnetization and coercivity values of 4.6×10^5 A/m and 0.6 mT, respectively. Magnetic energy density on the surface of oriented particles was determined by $B^2/2\mu_0$ (B is the magnetic field and μ_0 is the vacuum permeability), as well as to obtain the energy landscape over the particles (the height to the particle top is 1 μm).

Static bending simulations of the gelatin beams were performed based on the magnetic torque model from the magnetization

measurements and the Ogden hyperelastic material model (parameter $N = 1$) with a shear modulus μ of 0.85 kPa and a strain hardening exponent α of 9.28 (50), which were derived directly from the AFM measurements (fig. S5, A to C). The shape deformation simulation of the 2D particle network was also performed with this set of measured parameters (fig. S14). The swelling ratio of the hydrogel beam had an average value around 29% during the experiments (fig. S6), which was included to the beam geometries in the shape deformation simulations.

Preparation of cells

THP-1 [ATCC (American Type Culture Collection) TIB-202] monocyte cells were purchased from ATCC as a frozen vial. The cells were cultured in 75 cm^2 polystyrene cell culture flasks with 10% fetal bovine serum, 2-mM L-glutamine, and 1% penicillin/streptomycin containing Dulbecco's modified Eagle's medium. Suspension cells were diluted 1:2 and 1:3 for splitting. Before manipulation, cells were fixed with 2% glutaraldehyde/PBS solution.

SUPPLEMENTARY MATERIALS

Supplementary material for this article is available at <http://advances.sciencemag.org/cgi/content/full/7/23/eabe8436/DC1>

REFERENCES AND NOTES

- L. Hines, K. Petersen, G. Z. Lum, M. Sitti, Soft actuators for small-scale robotics. *Adv. Mater.* **29**, 1603483 (2017).
- C. Hu, S. Pané, B. J. Nelson, Soft micro- and nanorobotics. *Annu. Rev. Control Robot. Auton. Syst.* **1**, 53–75 (2018).
- S. Palagi, P. Fischer, Bioinspired microrobots. *Nat. Rev. Mater.* **3**, 113–124 (2018).
- Y. Zhang, F. Zhang, Z. Yan, Q. Ma, X. Li, Y. Huang, J. A. Rogers, Printing, folding, and assembly methods for forming 3D mesostructures in advanced materials. *Nat. Rev. Mater.* **2**, 17019 (2017).
- A. Rafsanjani, K. Bertoldi, A. R. Studart, Programming soft robots with flexible mechanical metamaterials. *Sci. Robot.* **4**, eaav7874 (2019).
- B. Zhang, A. Korolj, B. F. L. Lai, M. Radisic, Advances in organ-on-a-chip engineering. *Nat. Rev. Mater.* **3**, 257–278 (2018).
- S. Tasoglu, E. Diller, S. Guven, M. Sitti, U. Demirci, Untethered micro-robotic coding of three-dimensional material composition. *Nat. Commun.* **5**, 3124 (2014).
- M. Sitti, Miniature soft robots—Road to the clinic. *Nat. Rev. Mater.* **3**, 74–75 (2018).
- H. Ceylan, I. C. Yasa, O. Yasa, A. F. Tabak, J. Giltinan, M. Sitti, 3D-printed biodegradable microswimmer for theranostic cargo delivery and release. *ACS Nano* **13**, 3353–3362 (2019).
- H. Ceylan, I. C. Yasa, U. Kilic, W. Hu, M. Sitti, Translational prospects of untethered medical microrobots. *Prog. Biomed. Eng.* **1**, 012002 (2019).
- J. Kim, S. E. Chung, S.-E. Choi, H. Lee, J. Kim, S. Kwon, Programming magnetic anisotropy in polymeric microactuators. *Nat. Mater.* **10**, 747–752 (2011).
- H.-W. Huang, M. S. Sakar, A. J. Petruska, S. Pané, B. J. Nelson, Soft micromachines with programmable motility and morphology. *Nat. Commun.* **7**, 12263 (2016).
- H. Lu, M. Zhang, Y. Yang, Q. Huang, T. Fukuda, Z. Wang, Y. Shen, A bioinspired multilegged soft millirobot that functions in both dry and wet conditions. *Nat. Commun.* **9**, 3944 (2018).
- S. R. Goudo, I. C. Yasa, X. Hu, H. Ceylan, W. Hu, M. Sitti, Biodegradable untethered magnetic hydrogel milli-grippers. *Adv. Funct. Mater.* **30**, 2004975 (2020).
- Y. Kim, G. A. Parada, S. Liu, X. Zhao, Ferromagnetic soft continuum robots. *Sci. Robot.* **4**, eaax7329 (2019).
- W. Hu, G. Z. Lum, M. Mastrangeli, M. Sitti, Small-scale soft-bodied robot with multimodal locomotion. *Nature* **554**, 81–85 (2018).
- Z. Ren, W. Hu, X. Dong, M. Sitti, Multi-functional soft-bodied jellyfish-like swimming. *Nat. Commun.* **10**, 2703 (2019).
- Y. Kim, H. Yuk, R. Zhao, S. A. Chester, X. Zhao, Printing ferromagnetic domains for untethered fast-transforming soft materials. *Nature* **558**, 274–279 (2018).
- T. Xu, J. Zhang, M. Salehizadeh, O. Onaizah, E. Diller, Millimeter-scale flexible robots with programmable three-dimensional magnetization and motions. *Sci. Robot.* **4**, eaav4494 (2019).
- J. Palacci, S. Sacanna, A. P. Steinberg, D. J. Pine, P. M. Chaikin, Living crystals of light-activated colloidal surfers. *Science* **339**, 936–940 (2013).
- R. M. Erb, H. S. Son, B. Samanta, V. M. Rotello, B. B. Yellen, Magnetic assembly of colloidal superstructures with multipole symmetry. *Nature* **457**, 999–1002 (2009).

22. K. Han, C. W. Shields IV, N. M. Diwakar, B. Bharti, G. P. López, O. D. Velev, Sequence-encoded colloidal origami and microbot assemblies from patchy magnetic cubes. *Sci. Adv.* **3**, e1701108 (2017).
23. F. Ma, S. Wang, D. T. Wu, N. Wu, Electric-field-induced assembly and propulsion of chiral colloidal clusters. *Proc. Natl. Acad. Sci. U.S.A.* **112**, 6307–6312 (2015).
24. Y. Alapan, B. Yigit, O. Beker, A. F. Demirörs, M. Sitti, Shape-encoded dynamic assembly of mobile micromachines. *Nat. Mater.* **18**, 1244–1251 (2019).
25. F. Martinez-Pedrero, A. Ortiz-Ambriz, I. Pagonabarraga, P. Tierno, Colloidal microworms propelling via a cooperative hydrodynamic conveyor belt. *Phys. Rev. Lett.* **115**, 138301 (2015).
26. T. O. Tasci, P. S. Herson, K. B. Neeves, D. W. M. Marr, Surface-enabled propulsion and control of colloidal microwheels. *Nat. Commun.* **7**, 10225 (2016).
27. A. Aubret, M. Youssef, S. Sacanna, J. Palacci, Targeted assembly and synchronization of self-spinning microgears. *Nat. Phys.* **14**, 1114–1118 (2018).
28. A. Snezhko, I. S. Aranson, Magnetic manipulation of self-assembled colloidal asters. *Nat. Mater.* **10**, 698–703 (2011).
29. R. Dreyfus, J. Baudry, M. L. Roper, M. Fermigier, H. A. Stone, J. Bibette, Microscopic artificial swimmers. *Nature* **437**, 862–865 (2005).
30. T. Mirkovic, M. L. Foo, A. C. Arsenault, S. Fournier-Bidoz, N. S. Zacharia, G. A. Ozin, Hinged nanorods made using a chemical approach to flexible nanostructures. *Nat. Nanotechnol.* **2**, 565–569 (2007).
31. W. Gao, S. Sattayasamitsathit, K. M. Manesh, D. Weihs, J. Wang, Magnetically powered flexible metal nanowire motors. *J. Am. Chem. Soc.* **132**, 14403–14405 (2010).
32. B. Jang, E. Gutman, N. Stucki, B. F. Seitz, P. D. Wendel-García, T. Newton, J. Pokki, O. Ergeneman, S. Pané, Y. Or, B. J. Nelson, Undulatory locomotion of magnetic multilink nanoswimmers. *Nano Lett.* **15**, 4829–4833 (2015).
33. J. Cui, T.-Y. Huang, Z. Luo, P. Testa, H. Gu, X.-Z. Chen, B. J. Nelson, L. J. Heyderman, Nanomagnetic encoding of shape-morphing micromachines. *Nature* **575**, 164–168 (2019).
34. J. Yan, S. C. Bae, S. Granick, Colloidal superstructures programmed into magnetic janus particles. *Adv. Mater.* **27**, 874–879 (2015).
35. J. Zhang, B. A. Grzybowski, S. Granick, Janus particle synthesis, assembly, and application. *Langmuir* **33**, 6964–6977 (2017).
36. A. Walther, A. H. E. Müller, Janus particles: Synthesis, self-assembly, physical properties, and applications. *Chem. Rev.* **113**, 5194–5261 (2013).
37. X. Hu, S. R. Torati, J. Yoon, B. Lim, K. Kim, C. Kim, Magnetically characterized molecular lubrication between biofunctionalized surfaces. *ACS Appl. Mater. Interfaces* **10**, 16177–16182 (2018).
38. S. C. Glotzer, M. J. Solomon, Anisotropy of building blocks and their assembly into complex structures. *Nat. Mater.* **6**, 557–562 (2007).
39. P. F. Damasceno, M. Engel, S. C. Glotzer, Predictive self-assembly of polyhedra into complex structures. *Science* **337**, 453–457 (2012).
40. T.-Y. Huang, H.-W. Huang, D. D. Jin, Q. Y. Chen, J. Y. Huang, L. Zhang, H. L. Duan, Four-dimensional micro-building blocks. *Sci. Adv.* **6**, eaav8219 (2020).
41. Z.-C. Ma, Y.-L. Zhang, B. Han, X.-Y. Hu, C.-H. Li, Q.-D. Chen, H.-B. Sun, Femtosecond laser programmed artificial musculoskeletal systems. *Nat. Commun.* **11**, 4536 (2020).
42. M. Hippler, E. Blasco, J. Qu, M. Tanaka, C. Barner-Kowollik, M. Wegener, M. Bastmeyer, Controlling the shape of 3D microstructures by temperature and light. *Nat. Commun.* **10**, 232 (2019).
43. X. Hu, B. Lim, S. R. Torati, J. Ding, V. Novosad, M.-Y. Im, V. Reddy, K. Kim, E. Jung, A. I. Shawl, E. Kim, C. Kim, Autonomous magnetic microrobots by navigating gates for multiple biomolecules delivery. *Small* **14**, 1800504 (2018).
44. X. Hu, S. R. Torati, H. Kim, J. Yoon, B. Lim, K. Kim, M. Sitti, C. Kim, Multifarious transit gates for programmable delivery of bio-functionalized matters. *Small* **15**, 1901105 (2019).
45. Y. Alapan, U. Bozuyuk, P. Erkoç, A. C. Karacakol, M. Sitti, Multifunctional surface microrollers for targeted cargo delivery in physiological blood flow. *Sci. Robot.* **5**, eaba5726 (2020).
46. S. Sun, Recent advances in chemical synthesis, self-assembly, and applications of FePt nanoparticles. *Adv. Mater.* **18**, 393–403 (2006).
47. S.-W. Chou, Y.-H. Shau, P.-C. Wu, Y.-S. Yang, D.-B. Shieh, C.-C. Chen, In vitro and in vivo studies of FePt nanoparticles for dual modal CT/MRI molecular imaging. *J. Am. Chem. Soc.* **132**, 13270–13278 (2010).
48. M. Muzzio, J. Li, Z. Yin, I. Michael Delahunty, J. Xie, S. Sun, Monodisperse nanoparticles for catalysis and nanomedicine. *Nanoscale* **11**, 18946–18967 (2019).
49. P. Bender, A. Günther, A. Tschöpe, R. Birringer, Synthesis and characterization of uniaxial ferrogels with Ni nanorods as magnetic phase. *J. Magn. Magn. Mater.* **323**, 2055–2063 (2011).
50. M. Czerner, L. S. Fellay, M. P. Suárez, P. M. Frontini, L. A. Fasce, Determination of elastic modulus of gelatin gels by indentation experiments. *Proc. Mater. Sci.* **8**, 287–296 (2015).

Acknowledgments: We thank F. Thiele and B. Ludescher for helping with magnetron sputtering, A. Shiva and N. Krishna-Subbaiah for helping with Nanoscribe 3D printing, R. Soon for helping with the custom electromagnetic coil setup, and O. Yasa for helping with the nanoindentation characterization. **Funding:** X.H. was supported by the Alexander von Humboldt Foundation. This work was funded by the Max Planck Society, European Research Council (ERC) Advanced Grant SoMMoR project with grant no. 834531, and German Research Foundation (DFG) Soft Material Robotic Systems (SPP 2100) Program with grant no. 2197/3-1. **Author contributions:** X.H., I.C.Y., H.C., W.H., and M.S. conceived and planned the research. X.H. performed the experiments and analyzed the data. I.C.Y., Z.R., S.R.G., H.C., and W.H. assisted with the experiments. Z.R., X.H., and W.H. performed the deformation simulations; S.R.G. performed the magnetic domain simulations. X.H. wrote the manuscript with contributions from all authors. M.S. supervised the project. **Competing interests:** The authors declare that they have no competing interests. **Data and materials availability:** All data needed to evaluate the conclusions in the paper are present in the paper and/or the Supplementary Materials.

Submitted 17 September 2020

Accepted 20 April 2021

Published 4 June 2021

10.1126/sciadv.abe8436

Citation: X. Hu, I. C. Yasa, Z. Ren, S. R. Goudou, H. Ceylan, W. Hu, M. Sitti, Magnetic soft micromachines made of linked microactuator networks. *Sci. Adv.* **7**, eabe8436 (2021).

Magnetic soft micromachines made of linked microactuator networks

Xinghao Hu, Immihana C. Yasa, Ziyu Ren, Sandhya R. Gouda, Hakan Ceylan, Wenqi Hu and Metin Sitti

Sci Adv 7 (23), eabe8436.

DOI: 10.1126/sciadv.abe8436

ARTICLE TOOLS

<http://advances.sciencemag.org/content/7/23/eabe8436>

SUPPLEMENTARY MATERIALS

<http://advances.sciencemag.org/content/suppl/2021/05/28/7.23.eabe8436.DC1>

REFERENCES

This article cites 50 articles, 5 of which you can access for free
<http://advances.sciencemag.org/content/7/23/eabe8436#BIBL>

PERMISSIONS

<http://www.sciencemag.org/help/reprints-and-permissions>

Use of this article is subject to the [Terms of Service](#)

Science Advances (ISSN 2375-2548) is published by the American Association for the Advancement of Science, 1200 New York Avenue NW, Washington, DC 20005. The title *Science Advances* is a registered trademark of AAAS.

Copyright © 2021 The Authors, some rights reserved; exclusive licensee American Association for the Advancement of Science. No claim to original U.S. Government Works. Distributed under a Creative Commons Attribution License 4.0 (CC BY).